

Gamma-ray Burst Prompt Emission Spectrum and E_p Evolution Patterns in the ICMART Model

XUEYING SHAO¹ AND HE GAO¹

¹*Department of Astronomy, Beijing Normal University, Beijing 100875, China*

ABSTRACT

In this paper, we simulate the gamma-ray bursts (GRBs) prompt emission light curve, spectrum and E_p evolution patterns within the framework of the Internal-Collision-induced MAgnetic Reconnection and Turbulence (ICMART) model. We show that this model can produce a Band shape spectrum, whose parameters (E_p , α , β) could distribute in the typical distribution from GRB observations, as long as the magnetic field and the electron acceleration process in the emission region are under appropriate conditions. On the other hand, we show that for one ICMART event, E_p evolution is always a hard-to-soft pattern. However, a GRB light curve is usually composed of multiple ICMART events that are fundamentally driven by the erratic GRB central engine activity. In this case, we find that if one individual broad pulse in the GRB light curve is composed of multiple ICMART events, the overall E_p evolution could be disguised as the intense-tracking pattern. Therefore, mixed E_p evolution patterns can coexist in the same burst, with a variety of combined patterns. Our results support the ICMART model to be a competitive model to explain the main properties of GRB prompt emission. The possible challenges faced by the ICMART model are also discussed in details.

1. INTRODUCTION

Gamma-ray bursts (GRBs) are the most luminous explosions in the universe. Their bursty emission in the hard-X-ray/soft- γ -ray band is usually called the “prompt emission” (Zhang 2018). The temporal structure of the prompt emission exhibits diverse morphologies (Fishman & Meegan 1995), which can vary from a single smooth pulse to extremely complex light curves with many pulses overlapping within a short duration. Gao et al. (2012) proposed that the prompt emission light curves are typically the superposition of an underlying slow component and a more rapid fast component, where the fast component tends to be more significant in high energies and becomes less significant at lower frequencies (Vetere et al. 2006).

The photon number spectrum of prompt emission, both for time-resolved spectrum and time-integrated spectrum, can usually be fitted with a broken power law known as the Band function (Band et al. 1993)

$$N(E) = \begin{cases} A \left(\frac{E}{100\text{keV}}\right)^\alpha e^{-E/E_0} & , E < (\alpha - \beta)E_0 \\ A \left[\frac{(\alpha - \beta)E_0}{100\text{keV}}\right]^{\alpha - \beta} e^{\beta - \alpha} \left(\frac{E}{100\text{keV}}\right)^\beta & , E \geq (\alpha - \beta)E_0 \end{cases} \quad (1)$$

where A is the normalization factor, E_0 is the break energy in the spectrum, α and β are the low-energy and high-energy photon spectral indices with α ranging at $(-2, 0)$ and β ranging at $(-4, -1)$ (Preece et al. 2000). The peak energy of the $E^2 N(E)$ spectrum ($E_p = (2 + \alpha)E_0$) distributes within several orders of magnitude but clusters around 200 – 300keV (Preece et al. 2000; Goldstein et al. 2013). For bright bursts, two types of evolution patterns between E_p and flux are usually observed, i.e. the hard-to-soft pattern (Norris et al. 1986) where E_p decreases throughout the pulse and the intensity-tracking pattern (Kargatis et al. 1994; Bhat et al. 1994; Golenetskii et al. 1983) where E_p tracks the radiation intensity.

After decades of investigations, the origin of GRB prompt emission is still under debated. The main obstacle in front of theorists is the composition of GRB outflows. For matter-dominated scenario, the most representative model is the so-called the internal shock model (Rees & Meszaros 1994). In this model, a relativistic unsteady outflow is generated from the central engine, which can be represented as a succession of shells ejected with random velocity, mass and

width. Mechanical collisions between the faster late shells and the slower early shells could convert a certain fraction of the relative kinetic energy into internal energy by the resulting internal shocks. The internal energy thus generated is then radiated via synchrotron or inverse Compton scattering and giving rise to the prompt emission. In this scenario, the non-thermal spectrum is naturally expected as long as the collision radius is beyond the photosphere radius, and the temporal variability is attributed to the erratic activity of the central engine while the angular spreading time of shells at different radius causes the variable timescales (Rees & Meszaros 1994; Kobayashi et al. 1997). This model is difficult to account for superposed slow and fast variability components, unless the central engine itself carries these two variability components in the time history of jet launching, which has no proper explanation in physics (Hascoët et al. 2012). For the evolution patterns between E_p and flux, the internal shock model is easy to explain intensity-tracking pattern, but difficult to interpret the hard to soft pattern. In addition, the internal shock model also faces other challenges (Zhang & Yan 2011, for a review), including the efficiency problem (Panaitescu et al. 1999; Kumar 1999), fast cooling problem (Ghisellini et al. 2000; Kumar & McMahon 2008), the electron number excess problem (Daigne & Mochkovitch 1998; Shen & Zhang 2009), the missing bright photosphere problem (Zhang & Pe’Er 2009; Daigne & Mochkovitch 2002) and so on.

In order to solve these problems, people proposed that GRB outflows should be Poynting flux dominated instead of matter-dominated. Significant magnetic dissipation may happen to power GRB prompt emission through different mechanisms, including MHD-condition-broken scenarios (Usov 1994; Zhang & Mészáros 2002), radiation-dragged dissipation model (Mészáros & Rees 1997), the slow dissipation model (Thompson 1994; Drenkhahn & Spruit 2002; Giannios 2008; Beniamini & Giannios 2017), current-driven instabilities (Lyutikov & Blandford 2003), and forced magnetic reconnection (Zhang & Yan 2011; McKinney & Uzdensky 2012; Lazarian et al. 2019). In this work, we focus on one representative model, i.e., the Internal-Collision-induced MAGnetic Reconnection and Turbulence (ICMART) model (Zhang & Yan 2011). This model invokes a central engine powered, magnetically dominated outflow with magnetization factor $\sigma > 1$. Similar to the internal shock model, mechanical collisions between mini-shells would distort the ordered magnetic field and trigger fast magnetic seeds, which would induce relativistic magnetohydrodynamics (MHD) turbulence in the interaction regions¹. The turbulence further distorts the magnetic lines, resulting in a reconnection cascade and thus a significant release of the stored magnetic field energy (an ICMART event). The particles, either accelerated directly in the reconnection region or accelerated randomly in the turbulence region, would radiate synchrotron radiation photons to power the observed GRB prompt emission.

A global simulation of an ICMART event has been presented in Deng et al. (2015), which shows significant energy dissipation when two highly magnetized blobs collide. Mini-jet-like reconnection events are seen from the simulation, even though local simulations are needed to display mini-jets in much smaller scales. On the other hand, Monte Carlo simulations have been performed to simulate the prompt emission light curves within the framework of the ICMART model (Zhang & Zhang 2014). They show that the ICMART model can produce highly variable light curves with both fast and slow components, where the fast component is caused by many local Doppler-boosted mini-jets due to turbulent magnetic reconnection and the slow component is due to the runaway growth and subsequent depletion of these mini-jets. However, since these simulations were focusing on the temporal structure, they assumed that the radiation intensity arising from each reconnection event had the same spectral form (e.g., Band function with $\alpha = -1$, $\beta = -3$ and $E_p = 300\text{keV}$ in the observer frame), which made them ineffective in testing prompt emission spectrum properties.

In this work, we will further revise the previous simulation, by considering the evolution of the magnetic field with respect to radius and using a fast-cooling synchrotron spectrum to calculate the energy spectrum for each reconnection event, in order to judge whether the ICMART model could generate the Band spectrum and interpret the observed E_p evolution patterns.

2. SIMULATION METHODS

Within the ICMART scenario, a highly magnetized central engine would eject an unsteady outflow with variable Lorentz factors and luminosities but a nearly constant degree of magnetization. For simplicity, the outflow can be represented as a succession of discrete shells with variable Lorentz factors. Mechanical collisions between mini-shells would distort the magnetic field configurations and induce MHD turbulence, which will further distort the magnetic field and eventually trigger an ICMART event. Our simulation starts with tracking a shell with mass M_{bulk} , Lorentz

¹ It is worth noticing that rather than the mechanical collisions, the kink instability may be the cause of the magnetic turbulence but the physics processes they involve are similar (Lazarian et al. 2019).

factor Γ_0 and magnetized factor $\sigma_0 = E_{m,0}/E_{k,0}$ ($E_{m,0}$ marks the initial magnetic energy and $E_{k,0}$ marks the initial kinetic energy), when the shell expands to radius R_0 and the reconnection cascade has been triggered.

Numerical simulations have shown that the reconnection-driven magnetized turbulence could self-generate additional reconnections (Takamoto et al. 2015; Kowal et al. 2017; Takamoto 2018), inferring that the number of magnetic reconnections would increase exponentially. Here we assume that each reconnection event ejects a bipolar outflow and triggers two more reconnection events² (Zhang & Zhang 2014). Assuming the generation number of magnetic reconnections within the $1/\Gamma_0$ cone is n_g , the total number of magnetic reconnections N_{cone} could be estimated as $N_{\text{cone}} \approx \sum_{n=1}^{n_g} 2^n$. The duration for each reconnection in the lab frame could be estimated as

$$T_{r, \text{lab}} \sim \Gamma_0 \frac{L'}{v'_{\text{in}}} = 10^4 \text{s} \left(\frac{\Gamma_0}{100} \right) \left(\frac{L'}{10^{11} \text{cm}} \right) \left(\frac{v'_{\text{in}}}{10^9 \text{cm/s}} \right)^{-1}, \quad (2)$$

where L' is the size of the magnetic reconnection and v'_{in} is the inflow velocity of the magnetic field line. Hereafter, parameters denoted with ($'$) are in the rest frame of the jet bulk. Note that this duration timescale is about $T_{r, \text{obs}} \sim 0.1\text{s}$ in the observer frame and therefore the reconnections cascade lasts for $n_g T_{r, \text{obs}}$ in the observer frame.

For each reconnection event, the magnetized factor of the reconnection area drops from σ_0 to 1. Thus the dissipated magnetic energy approximately equals to $(\sigma_0 - 1)/\sigma_0$ times the magnetic energy within the reconnection area. We assume that half of the dissipated magnetic energy is used to boost the kinetic energy of the jet and the other half is initially distributed to electrons (Drenkhahn & Spruit 2002), and then gets converted to photons through synchrotron radiation. Part of the photons that beams toward the observer is recorded as the prompt emission of GRB.

In order to simulate the observed GRB spectrum, three rest frames need to be invoked: 1) the rest frame of the jet bulk; 2) the rest frame of the mini-jet; 3) the rest frame of the observer (here we ignore the cosmological expansion effect). Hereafter, parameters denoted with ($''$) are in the rest frame of the mini-jet. The quantities within these three frames are connected through two Doppler factors, i.e.,

$$\mathcal{D}_1 = [\Gamma(1 - \beta_{\text{bulk}} \cos \theta)]^{-1}, \quad (3)$$

$$\mathcal{D}_2 = [\gamma(1 - \beta \cos \phi)]^{-1}, \quad (4)$$

where $\gamma \approx \sqrt{1 + \sigma}$ is the relative Lorentz factor of mini-jet with respect to the jet bulk (Zhang & Zhang 2014), β_{bulk} and β are the corresponding dimensionless velocities with respect to Γ and γ , θ is the latitude of the mini-jet, i.e., the angle between the line of sight and the direction of the bulk at the location of the mini-jet and ϕ is the angle between the direction of the mini-jet and the direction of the bulk in the bulk comoving frame. In our simulation, we trace each mini-jet to calculate its radiation intensity and photon energy distribution in the direction of the observer, and stack the simultaneously arriving photons from all mini-jets to obtain the overall light curve and the corresponding time-resolved spectrum.

In the rest frame of the mini-jet, synchrotron radiation power at frequency ν'' is given by (Rybicki & Lightman 1979)

$$P''_{\nu''} = \frac{\sqrt{3} q_e^3 B_e''}{m_e c^2} \int_{\gamma_{e,m}}^{\gamma_{e,M}} \left(\frac{dN_e''}{d\gamma_e} \right) F \left(\frac{\nu''}{\nu''_{\text{cr}}} \right) d\gamma_e, \quad (5)$$

where q_e is electron charge, $\nu''_{\text{cr}} = 3\gamma_e^2 q_e B_e'' / (4\pi m_e c)$ is the characteristic frequency of an electron with Lorentz factor γ_e , B_e'' is the comoving magnetic field strength in the emission region and $F(x) = x \int_x^\infty K_{5/3}(\xi) d\xi$ with $K_{5/3}(x)$ is the modified Bessel Function of five thirds order. Lacking full numerical simulations of magnetic turbulence and reconnection, the comoving magnetic field strength B_e'' in the mini-jet is rather difficult to make a direct estimation. Here we introduce a free parameter k to connect B_e'' with the bulk magnetic field strength as $B_e'' = \sqrt{k} B' / \gamma$. The value of k is justified by limiting E_p in the simulation results to be consistent with the observational data. We assume B_e'' decays with the radius of the bulk as

$$B_e''(R) = B''_{e,0} \left(\frac{R}{R_0} \right)^{-b}, \quad (6)$$

where b would be much larger than 1, due to the rapid consumption of magnetic energy in the reconnection process. Considering the magnetic flux conservation, the bulk magnetic field strength B' decreases as the jet expanding. The

² Lacking detailed numerical simulations for a reconnection/turbulence cascade, the specific index of magnetic reconnection growth is still unknown. Here we assume each reconnection would trigger two more new reconnection events. The uncertainty brought by this assumption will not affect our analysis results about spectrum and E_p evolution (because these results are already the superposition effect of sufficient magnetic reconnection events), but might affect the time when our simulated light curve would reach the peak.

radial part of the magnetic field decreases as $B'_r \propto R^{-2}$ while the transverse part decreases as $B'_t \propto R^{-1}$. At a large radius one has a transverse-dominated magnetic field

$$B'(R) = B'_0 \left(\frac{R}{R_0}\right)^{-1}, \quad (7)$$

where B'_0 is the initial magnetic strength of the bulk.

The electrons number density could be estimated with the continuity equation (Uhm & Zhang 2014):

$$\frac{\partial N''(\gamma_e, t'')}{\partial t''} = -\frac{\partial}{\partial \gamma_e} [\dot{\gamma}_e(\gamma_e) N''(\gamma_e, t'')] + Q(\gamma_e, t''), \quad (8)$$

where $\dot{\gamma}_e(\gamma_e)$ denotes the electron cooling rate and $Q(\gamma_e, t'')$ denotes the injected source function. Electrons would suffer both radiative and adiabatic cooling (Uhm & Zhang 2014), so that

$$\frac{d}{dt''} \left(\frac{1}{\gamma_e}\right) = \frac{\sigma_T B_e''^2}{6\pi m_e c} + \frac{2}{3} \left(\frac{1}{\gamma_e}\right) \frac{d \ln R}{dt''}, \quad (9)$$

where σ_T is the Thomson scattering cross section. The distribution of the accelerated electrons is usually assumed to be a power-law function,

$$Q(\gamma_e) = Q_0 \left(\frac{\gamma_e}{\gamma_{e,m}}\right)^{-p}, \quad \gamma_{e,m} < \gamma_e < \gamma_{e,M}, \quad (10)$$

where Q_0 is a normalization factor, $\gamma_{e,m}$ and $\gamma_{e,M}$ are the minimum and maximum injected electron Lorentz factor. $\gamma_{e,M}$ could be calculated as

$$\gamma_{e,M} = \sqrt{\frac{6\pi q_e}{\sigma_T B_e''}}. \quad (11)$$

One can use electron number and energy conservation law to solve Q_0 and $\gamma_{e,m}$ for a specific reconnection event, which should require

$$Q_0(t''_e - t''_s) \int_{\gamma_m}^{\gamma_M} \left(\frac{\gamma_e}{\gamma_m}\right)^{-p} d\gamma_e = f_e \int_{t''_s}^{t''_e} L'^2 v'_{in} n'_e dt', \quad (12)$$

and

$$\frac{1}{2} \delta E'_{p, inj} = \int_{t''_s}^{t''_e} \int_{\gamma_m}^{\gamma_M} Q_0 \left(\frac{\gamma_e}{\gamma_m}\right)^{-p} d\gamma_e dt'' (\gamma_e - 1) m_e c^2, \quad (13)$$

where t_s and t_e are the starting and ending time of the magnetic reconnection, f_e is the fraction of accelerated electrons within the reconnection area, $n'_e \propto R^{-2}$ is the number density of electrons in the bulk frame, and $\delta E'_{p, inj}$ is the dissipated energy for a single magnetic reconnection, which could be estimated as

$$\delta E'_{p, inj} = \frac{\sigma_0 - 1}{\sigma_0} \int_{t'_s}^{t'_s + T'_0} \frac{B'(t)^2}{8\pi} L'(t)^2 v'_{in} dt', \quad (14)$$

where t'_s is the beginning time. Considering both the expansion and reconnection effects, similar to the bulk magnetic field strength, here we assume a general evolution form for L' ,

$$L'(R) = L'_0 \left(\frac{R}{R_0}\right)^l, \quad (15)$$

where L'_0 is the initial magnetic reconnection size.

As seen by the observer, each mini-jet radiation corresponds to a single pulse starting from t'_s/\mathcal{D}_1 to $(t'_s + T'_0)/\mathcal{D}_1$, with radiation power

$$P_\nu = \mathcal{D}_1^3 \mathcal{D}_2^3 P''_\nu. \quad (16)$$

As suggested by Zhang & Zhang (2014), here we use Gaussian shape to simulate each single pulse in the light curve. For a given time interval in the observer frame (t_1, t_2) , the time resolved spectrum is given by

$$P_\nu(\nu) = \sum_{N_{\text{cone}}} \sum_{t=t_1}^{t=t_2} P_\nu(\nu, t) \quad (17)$$

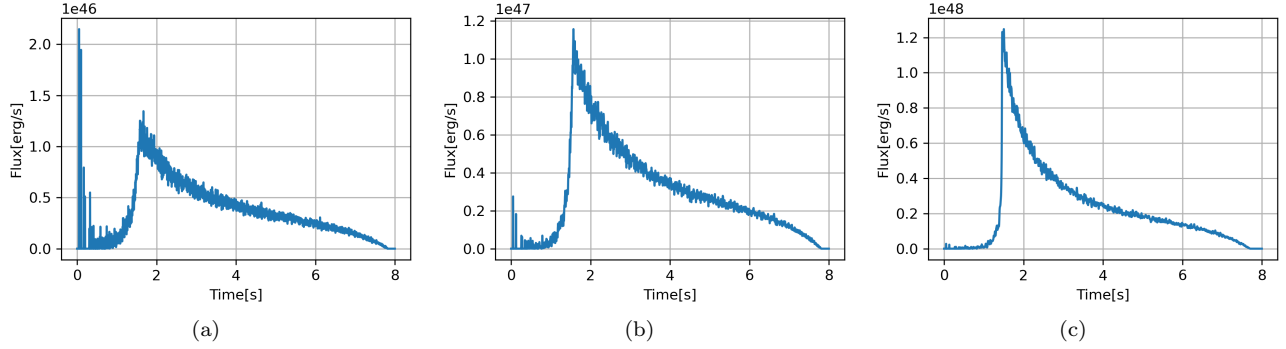


Figure 1. Simulated light curves of one ICMART event with the following parameters: (a) $l = 0.0$; (b) $l = 0.2$; (c) $l = 0.4$.

For one ICMART event, the peak time of the light curve corresponds to the total duration for the cascade process, which could be estimated as

$$T_p \sim \frac{R_f}{2\Gamma^2 c} \sim 1.5\text{s} \left(\frac{n_g}{10}\right) \left(\frac{\Gamma_0}{200}\right)^{-1} \left(\frac{L'}{10^{11}\text{cm}}\right) \left(\frac{v'_{\text{in}}}{10^9\text{cm/s}}\right)^{-1}. \quad (18)$$

We assume an abrupt cessation of the cascade process, so that the number of new mini-jets drops to 0. The light curve after T_p is therefore contributed by the high-latitude emission from other mini-jets not along the line of sight due to the “curvature effect” delay.

3. RESULTS

In order to justify whether the ICMART model could generate the Band spectrum and the observed E_p evolution patterns, we first run a series of simulation for one ICMART event with initial setup: $M_{\text{bulk}} \in \mathcal{U}(3.5 \times 10^{-9}, 3.5 \times 10^{-6})M_{\odot}$, $R_0 = 10^{14}\text{cm}$, $L'_0 = 1.2 \times 10^{11}\text{cm}$, $v'_{\text{in}} = 3 \times 10^9\text{cm/s}$, $n_g \in \mathcal{U}(13, 17)$, $\Gamma_0 \in \mathcal{U}(100, 300)$, $\sigma_0 \in \mathcal{U}(5, 50)$, $k \in \mathcal{U}(5 \times 10^{-8}, 5 \times 10^{-2})$, $p \in \mathcal{U}(2.3, 2.8)$, $f_e \in \mathcal{U}(0.01, 1)$, $b \in \mathcal{U}(1, 50)$, $l \in \mathcal{U}(0, 1)$, $\theta \in \mathcal{U}(0, 2/\Gamma_0)$ and $\phi \in \mathcal{U}(0, \frac{\pi}{2})$, where \mathcal{U} refers to the Uniform distribution. In figs. 1 to 6 we plot the simulation results for selected situations that are relevant for illustrating the main conclusions, which can be summarized in the following subsections.

3.1. Light Curve

In our simulation, each ICMART event would produce highly variable light curves, which can be decomposed as the superposition of an underlying slow component and a more rapid fast component. The fast component is related to the individual locally Doppler-boosted mini-emitters, while the slow component is caused by the superposition of emission from all the mini-jets in the emission region. The duration of each mini-pulse and the total duration of the light curve are essentially determined by the parameters related to the number and scale of magnetic reconnection, e.g., L'_0 , l , v'_{in} and n_g .

Our results are basically consistent with the previous simulation results from Zhang & Zhang (2014). It is worth pointing out that Zhang & Zhang (2014) did not invoke any real radiation process for each mini-jet, so they haven’t discussed the evolution effect of the magnetic field and the magnetic reconnection scale. In this work, we find that if the evolution of the magnetic reconnection scale is not introduced (i.e. $l = 0$), the radiation contributed by a single mini-jet in the early stage would be much larger than that in the late stage, due to the magnetic field decaying. Consequently, some short spikes (with flux equivalent to, or even larger than the main peak) would show up in the early stage of the light curve as shown in fig. 1. This phenomenon will disappear after introducing the evolution of reconnection scale with radius (e.g. $l > 0.2$).

3.2. Spectrum

For most cases, the spectrum produced by ICMART events would behave as broken power law, which could be well fitted with the Band function. For example, we plot the time resolved spectrum at 1 s and 3 s (in the observer frame) for one simulation ³ in fig. 2(a), in a narrower band pass from 3 keV to 3 MeV. In the example, the best fit

³ Here we would like to note that due to the randomness of θ and ϕ , for a given parameter combination, different simulations may give slightly different GRB light curve and spectrum, but the conclusions we show below are robust because the number of mini-jets is large enough to smooth out the main random effects.

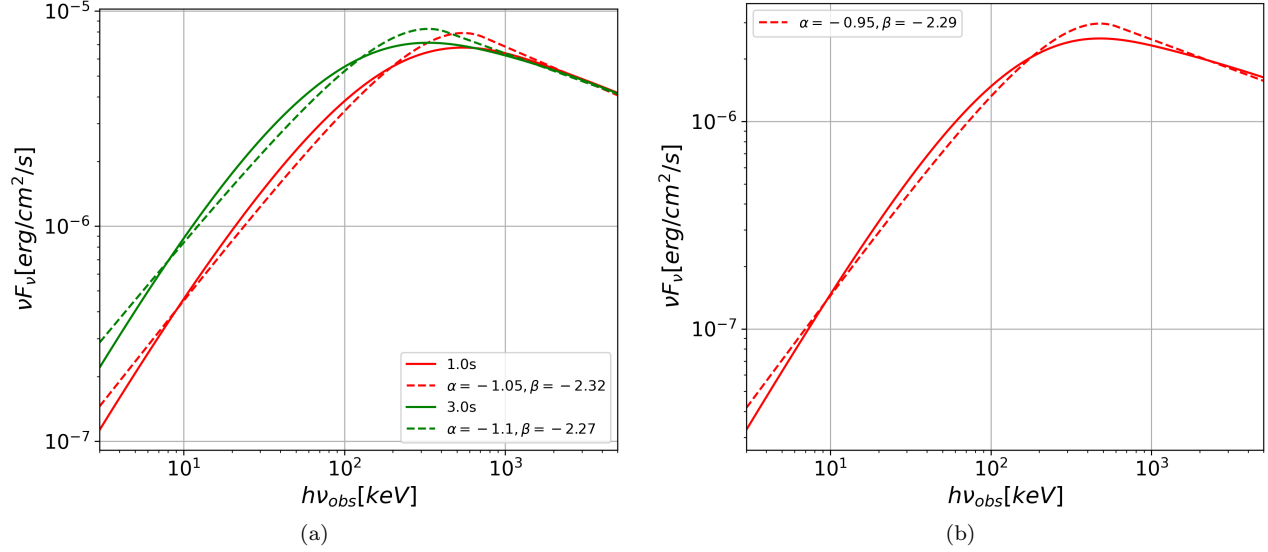


Figure 2. (a) Simulated spectrum of one ICMART event with the following parameters: $M_{\text{bulck}} = 3 \times 10^{-8} M_{\odot}$, $R_0 = 10^{14}$ cm, $L'_0 = 1.2 \times 10^{11}$ cm, $v'_{\text{in}} = 3 \times 10^9$ cm/s, $n_g = 15$, $\Gamma_0 = 200$, $\sigma_0 = 8$, $k = 5 \times 10^{-7}$, $p = 2.8$, $f_e = 0.1$, $b = 30$, $l = 0.2$. The red and green solid lines represent the simulated spectrum at 1 s and 3 s in the observer's frame, and the dashed lines represent their relevant best fitting results with Band function. (b) Simulated spectrum for a single magnetic reconnection with the same parameters as the left panel but θ and ϕ are taken as 0. The solid line represent the simulation result and the dashed line is the best fitting result with Band function.

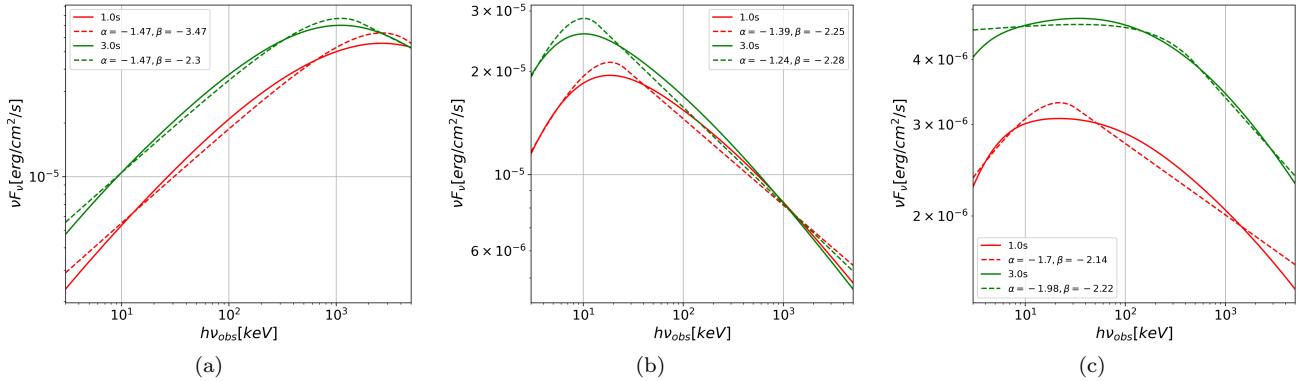


Figure 3. Simulated spectrum of one ICMART event with the following parameters: (a) $B''_e \approx 10^3$ G, $\gamma_{e,m} \approx 10^4$; (b) $B''_e \approx 500$ G, $\gamma_{e,m} \approx 10^3$; (c) $B''_e \approx 10$ G, $\gamma_{e,m} \approx 10^3$. Other parameters are the same as those in fig. 2(a).

parameters for Band function at 1s/3s are $\alpha = -1.05/-1.1$, $\beta = -2.32/-2.27$, and $E_p = 550/330$ keV, which are all typical values as suggested by the observations (Preece et al. 2000). This result is understandable since the observed spectrum is mainly shaped by the mini-jets that beam toward the observer, while as proven by Uhm & Zhang (2014), the radiation spectrum from mini-jets with $\theta = 0$ and $\phi = 0$ is very close to Band function (see fig. 2 for an example). The simulated spectrum may be slightly broader than the spectrum of a single reconnection, which should be caused by the contributions from off-axis mini-jets. However, the overall trend of the spectrum will not deviate too much from the Band spectrum.

Under the free combination of initial parameters, the E_p value of the simulated spectrum would distribute in a very wide range, much wider than the typical distribution from GRB observations (e.g., 3 keV \sim 3 MeV for current sample; Demianski et al. (2017)). In order to make 3 keV $< E_p <$ 3 MeV, a certain degeneracy is required between the initial parameters. For instance, since E_p is essentially proportional to $\Gamma_0 B''_e \gamma_m^2$ (Tavani 1996), the values of M_{bulck} , σ_0 , Γ_0 , R_0 , and k need cooperating to make the emission region magnetic field B''_e in the range of 10 \sim 10^4 G; on the other hand, the values of σ_0 and f_e need cooperating to make the minimum injected electron Lorentz factor $\gamma_{e,m}$ in the

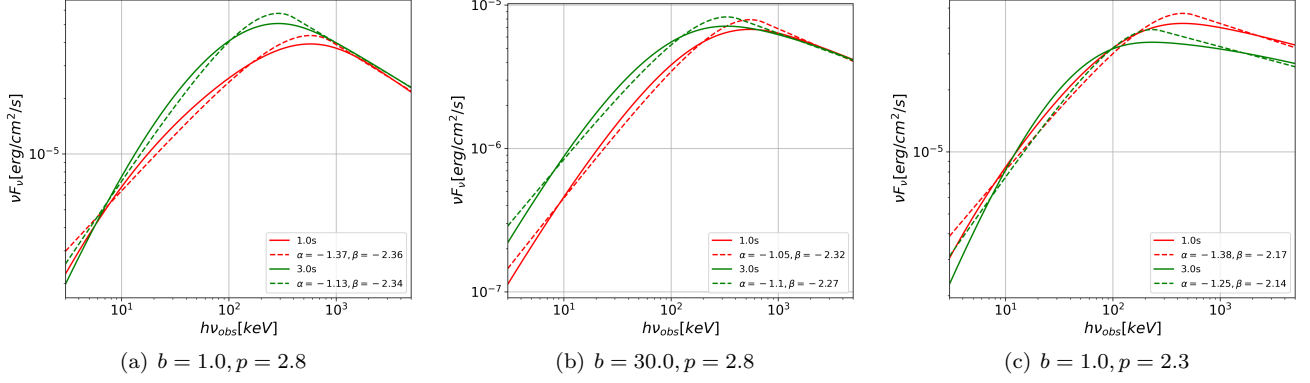


Figure 4. Simulated spectrum of one ICMART event with the following parameters: (a) $b = 1.0, p = 2.8$; (b) $b = 30.0, p = 2.8$; (c) $b = 1.0, p = 2.3$. Other parameters are the same as those in fig. 2(a).

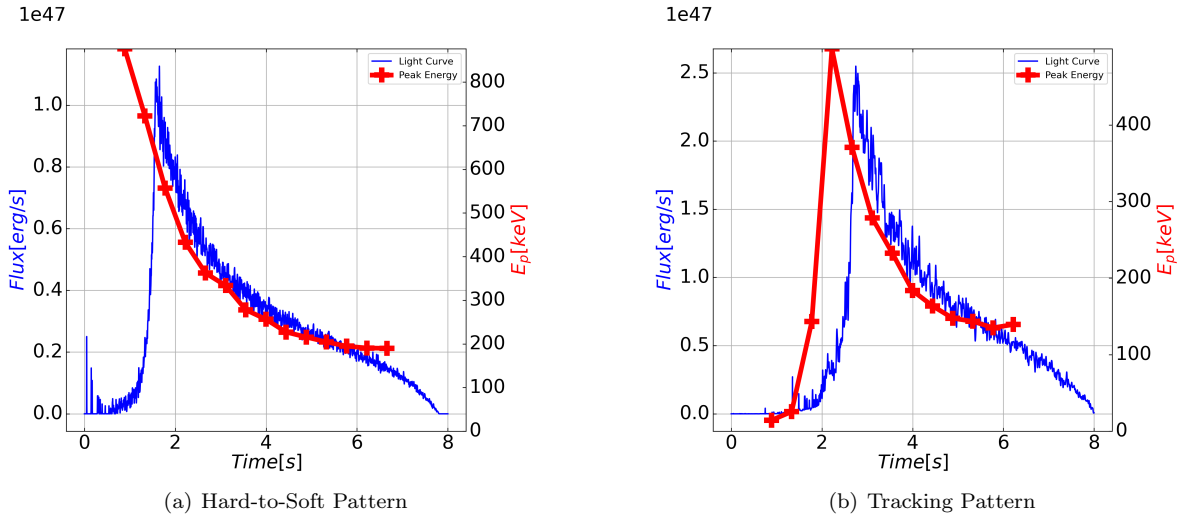


Figure 5. (a) Simulated E_p evolution of one ICMART event, with other parameters being the same as those in fig. 2(a). (b) Simulated E_p evolution of multiple ICMART events. The physical parameters for each ICMART event are listed in table 1.

range of $10^3 \sim 10^5$. Otherwise, E_p would be either higher (if B_e'' and/or $\gamma_{e,m}$ being too big) or lower (if B_e'' and/or $\gamma_{e,m}$ being too small) than typical GRB E_p distribution range (see figs. 3(a) and 3(b) for an example). Moreover, if the magnetic field in the radiation area is too small, the electrons would be cooled inefficiently, so the spectrum may deviate from the Band shape (see fig. 3(c) for an example).

For a Band-shape simulated spectrum, the higher spectral index (β) value is mainly determined by the injected electron energy distribution index (p), while the lower energy spectral index (α value) is essentially determined by the value of B_e'' and its evolution speed, which is reflected by the value of b (see fig. 4 for examples). When B_e'' is smaller than 1000G and b is larger than 30, α could be around -1 or even smaller, which is the typical value for current GRB observations. Otherwise, if B_e'' is too high or b is too small, α would approach -1.5 , entering the deep fast cooling regime for synchrotron radiation.

3.3. E_p Evolution

For one ICMART event, we find that the spectral peak E_p evolution is always a hard-to-soft pattern, namely E_p decreases throughout the whole event, even during the rising phase of the slow component, as shown in fig. 5(a). This is mainly because $E_p \propto B_e''$ and the magnetic field decreases with radius (and hence, time) as the shell expands in space. Our result is consistent with previous works (Uhm & Zhang 2016; Uhm et al. 2018), in which emitter are from a signal large emission region with decaying magnetic field.

$M_{\text{bulk}}(M_{\odot})$	f_e	k	n_g	σ_0	Γ_0	p	b	l	Start Time(s)
3×10^{-10}	1.0	5×10^{-4}	15	8	200	2.8	30	0.2	0.0
3×10^{-9}	0.3	1.5×10^{-5}	15	8	200	2.8	30	0.2	0.7
3×10^{-8}	0.1	5×10^{-7}	15	8	200	2.8	30	0.2	1.3

Table 1. Parameters for multiple ICMART events taken in the simulation of fig. 5(b).

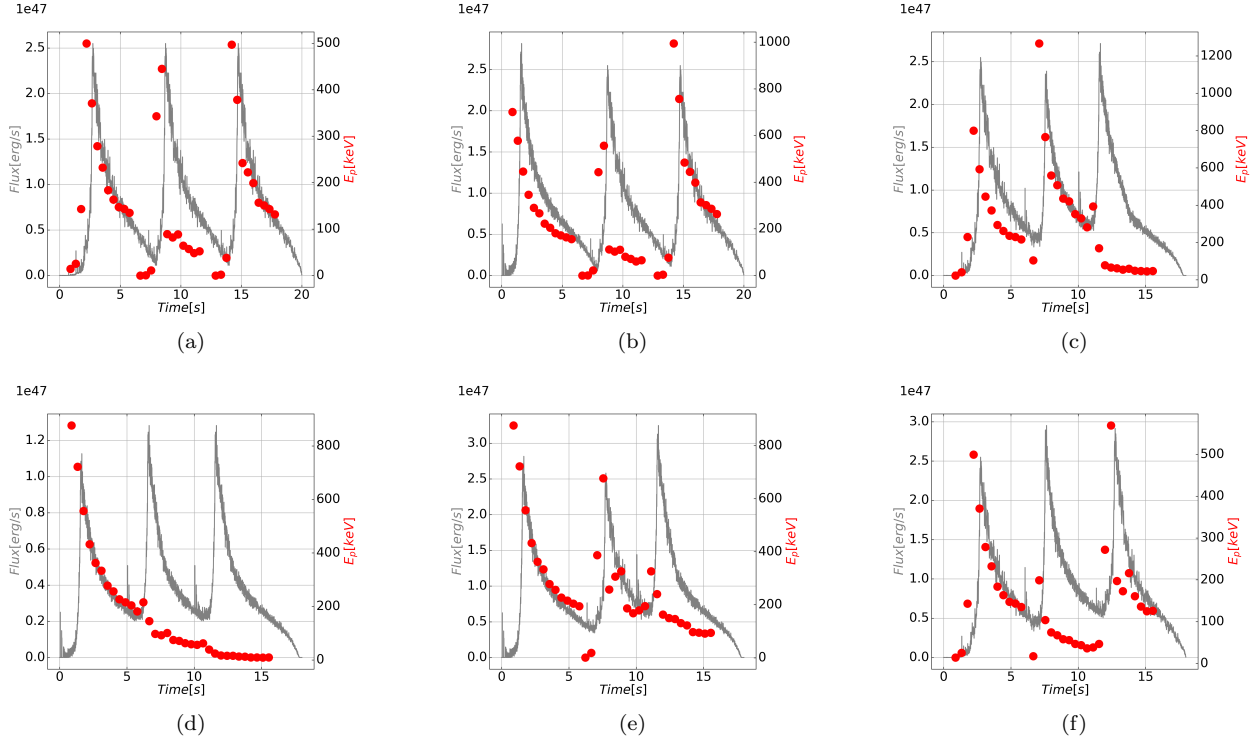


Figure 6. Simulation for different E_p evolution patterns by taking results in figs. 5(a) and 5(b) as templates: (a) overall intensity-tracking; (b) first hard-to-soft then intensity-tracking; (c) first intensity-tracking then hard-to-soft; (d) overall hard-to-soft; (e) and (f): two patterns appear alternately. The grey lines represent the light curves and the red spots represent the E_p value.

However, it is interesting to note that a GRB light curve is usually composed of multiple ICMART events that are fundamentally driven by the erratic GRB central engine activity. In this case, one broad component in real data is not necessarily generated by only one ICMART event. In fig. 5(b), we show an example light curve, which is generated with the superposition of three independent ICMART events. The physical parameters for each ICMART event are listed in table 1. Basically, by adjusting the parameters, we make the flux of the three events increase in turn over time. If the absolute value of E_p is positively correlated with flux, which seems to be supported by GRB observations (e.g., Amati/Yonetoku relations (Amati et al. 2002; Yonetoku et al. 2004)), the E_p evolution related to the overall light curve could be disguised as the intense-tracking pattern, namely E_p increases during the rising phase of the broad pulse and decreases during the falling phase.

If our interpretation is correct, this may explain why both types of E_p behavior are observed in individual GRB pulses. Furthermore, for one particular GRB whose light curve consists of multiple broad pulses, the E_p evolution for each broad pulse could be randomly hard-to-soft pattern or intense-tracking pattern. This could naturally explain why mixed E_p -evolution patterns can coexist in the same burst, with a variety of combined patterns (Lu et al. 2012).

For better illustration, we use the simulation results in fig. 5 as templates to simulate the E_p evolution and show that GRBs produced by multiple ICMART events could

1. have all pulses (including the first one) showings intensity-tracking behavior (see fig. 6(a));
2. have the first pulse showing a clear hard-to-soft evolution, while the rest of the pulses showing tracking behavior (see fig. 6(b));
3. have the first pulse showing a nice tracking behavior, but the later pulses showing a clear hard to soft evolution (see fig. 6(c));
4. have a overall hard to soft evolution (see fig. 6(d));
5. have two patterns appear alternately (see figs. 6(e) and 6(f)).

It is noticing that all these patterns have already been observed in the current GRB sample (Lu et al. 2012).

4. CONCLUSION AND DISCUSSION

The prompt emission of GRBs is still a mystery. The main uncertainty is the composition of the outflow, Poynting flux dominated or matter-dominated, which essentially determines the energy dissipation mechanism, particle acceleration mechanism, and radiation mechanism. Putting together all the observational evidence, including the properties of the light curve, the nature of the spectrum and the coordination between the spectrum and the light curve (e.g. the correlation between E_p and flux), may help to solve the problem.

In this work, we have developed a numerical code to simulate the prompt emission light curves, time resolved spectrum and E_p evolution patterns for GRBs produced by the Internal-Collision-induced MAGnetic Reconnection and Turbulence (ICMART) model. Our simulation results could be summarized as follows:

- The ICMART model could produce highly variable light curves, which can be decomposed as the superposition of an underlying slow component and a more rapid fast component. Such result is consistent with the previous simulations (Zhang & Zhang 2014) and the observation facts (Gao et al. 2012).
- The ICMART model could produce a Band shape spectrum, whose parameters (E_p , α , β) could distribute in the typical distribution from GRB observations, as long as the magnetic field and the electron acceleration process in the emission region are under appropriate conditions.
- For one ICMART event, the spectral peak E_p evolution is always hard-to-soft pattern. But if one individual broad pulse in the GRB light curve is composed of multiple ICMART events, the E_p evolution related to the overall light curve could be disguised as the intense-tracking pattern. Therefore, mixed E_p -evolution patterns can coexist in the same burst, with a variety of combined patterns.

Our results show that the ICMART model can explain the main characteristics of GRB light curve and spectrum, making it a very competitive model to produce GRB prompt emission. However, to interpret GRB observations in great detail, the ICMART model still faces some difficulties, which are worth pointing out.

In principle, the total energy and magnetic field strength carried by the shell of ICMART event can vary randomly in a wide range. However, in order to make GRBs from ICMART events, it is required that for all magnetic reconnection process, there is a preferred range for the magnetic field and the electron acceleration process in the emission region. Detailed numerical simulations of magnetic reconnection and particle acceleration processes are needed to address whether the B_e'' and $\gamma_{e,m}$ range demanded by the model could be achieved. One possibility is that the magnetic reconnection process is so intense that there is an upper limit on the strength of B_e'' (e.g. smaller than 10^4 G). It is worth noticing that for most GRBs, B_e'' can not reach this upper limit, but needs to be lower than 100 G and needs to decay very rapidly (down 1-2 orders of magnitude) during the radiation process, otherwise the lower energy index α for majority of GRBs would distribute around -1.5 (entering deep fast cooling regime), instead of around -1 as suggested by the observations.

It is possible that in some ICMART event, B_e'' is even lower than 10 G. For these cases, E_p of the spectrum would shift into the soft X-ray band. This might be the physical origin for the phenomenon so called ‘‘X-ray flashes (XRFs)’’, which are generally believed not to be a different population from GRBs, but rather the natural extension of GRBs

to the softer, less luminous regime (Sakamoto et al. 2008). Accumulated sample of more XRFs in the future with sky survey detectors in the X-ray band (e.g. Einstein Probe; (Yuan et al. 2018)) would help to justify this hypothesis.

ACKNOWLEDGMENTS

We thank helpful discussion with Bing Zhang. This work is supported by the National Natural Science Foundation of China (NSFC) under Grant No. 12021003.

REFERENCES

- Amati, L., Frontera, F., Tavani, M., et al. 2002, *Astronomy and Astrophysics*, 390, doi: [10.1051/0004-6361:20020722](https://doi.org/10.1051/0004-6361:20020722)
- Band, D., Matteson, J., Ford, L., et al. 1993, *The Astrophysical Journal*, 413, 281, doi: [10.1086/172995](https://doi.org/10.1086/172995)
- Beniamini, P., & Giannios, D. 2017, *MNRAS*, 468, 3202, doi: [10.1093/mnras/stx717](https://doi.org/10.1093/mnras/stx717)
- Bhat, P. N., Fishman, G. J., Meegan, C. A., et al. 1994, *The Astrophysical Journal*, 426, doi: [10.1086/174097](https://doi.org/10.1086/174097)
- Daigne, F., & Mochkovitch, R. 1998, *Monthly Notices of the Royal Astronomical Society*, 296, doi: [10.1046/j.1365-8711.1998.01305.x](https://doi.org/10.1046/j.1365-8711.1998.01305.x)
- . 2002, *Monthly Notices of the Royal Astronomical Society*, 336, doi: [10.1046/j.1365-8711.2002.05875.x](https://doi.org/10.1046/j.1365-8711.2002.05875.x)
- Demianski, M., Piedipalumbo, E., Sawant, D., & Amati, L. 2017, *A&A*, 598, A112, doi: [10.1051/0004-6361/201628909](https://doi.org/10.1051/0004-6361/201628909)
- Deng, W., Li, H., Zhang, B., & Li, S. 2015, *Astrophysical Journal*, 805, doi: [10.1088/0004-637X/805/2/163](https://doi.org/10.1088/0004-637X/805/2/163)
- Drenkhahn, G., & Spruit, H. C. 2002, *A&A*, 391, 1141, doi: [10.1051/0004-6361:20020839](https://doi.org/10.1051/0004-6361:20020839)
- Drenkhahn, G., & Spruit, H. C. 2002, *Astronomy and Astrophysics*, 391, 1141, doi: [10.1051/0004-6361:20020839](https://doi.org/10.1051/0004-6361:20020839)
- Fishman, G. J., & Meegan, C. A. 1995, *Annual Review of Astronomy and Astrophysics*, 33, 415, doi: [10.1146/annurev.aa.33.090195.002215](https://doi.org/10.1146/annurev.aa.33.090195.002215)
- Gao, H., Zhang, B.-B., & Zhang, B. 2012, *The Astrophysical Journal*, 748, 134, doi: [10.1088/0004-637X/748/2/134](https://doi.org/10.1088/0004-637X/748/2/134)
- Ghisellini, G., Celotti, A., & Lazzati, D. 2000, *Monthly Notices of the Royal Astronomical Society*, 313, doi: [10.1046/j.1365-8711.2000.03354.x](https://doi.org/10.1046/j.1365-8711.2000.03354.x)
- Giannios, D. 2008, *A&A*, 480, 305, doi: [10.1051/0004-6361:20079085](https://doi.org/10.1051/0004-6361:20079085)
- Goldstein, A., Preece, R. D., Mallozzi, R. S., et al. 2013, *Astrophysical Journal, Supplement Series*, 208, doi: [10.1088/0067-0049/208/2/21](https://doi.org/10.1088/0067-0049/208/2/21)
- Golenetskii, S. V., Mazets, E. P., Aptekar, R. L., & Ilyinskii, V. N. 1983, *Nature*, 306, doi: [10.1038/306451a0](https://doi.org/10.1038/306451a0)
- Hascoët, R., Daigne, F., & Mochkovitch, R. 2012, *Astronomy and Astrophysics*, 542, doi: [10.1051/0004-6361/201219339](https://doi.org/10.1051/0004-6361/201219339)
- Kargatis, V. E., Liang, E. P., Hurley, K. C., et al. 1994, *The Astrophysical Journal*, 422, doi: [10.1086/173724](https://doi.org/10.1086/173724)
- Kobayashi, S., Piran, T., & Sari, R. 1997, *The Astrophysical Journal*, 490, 92, doi: [10.1086/512791](https://doi.org/10.1086/512791)
- Kowal, G., Falceta-Gonçalves, D. A., Lazarian, A., & Vishniac, E. T. 2017, *ApJ*, 838, 91, doi: [10.3847/1538-4357/aa6001](https://doi.org/10.3847/1538-4357/aa6001)
- Kumar, P. 1999, *The Astrophysical Journal*, 523, doi: [10.1086/312265](https://doi.org/10.1086/312265)
- Kumar, P., & McMahon, E. 2008, *Monthly Notices of the Royal Astronomical Society*, 384, doi: [10.1111/j.1365-2966.2007.12621.x](https://doi.org/10.1111/j.1365-2966.2007.12621.x)
- Lazarian, A., Zhang, B., & Xu, S. 2019, *The Astrophysical Journal*, 882, doi: [10.3847/1538-4357/ab2b38](https://doi.org/10.3847/1538-4357/ab2b38)
- Lu, R. J., Wei, J. J., Liang, E. W., et al. 2012, *Astrophysical Journal*, 756, doi: [10.1088/0004-637X/756/2/112](https://doi.org/10.1088/0004-637X/756/2/112)
- Lyutikov, M., & Blandford, R. 2003, arXiv e-prints, astro. <https://arxiv.org/abs/astro-ph/0312347>
- McKinney, J. C., & Uzdensky, D. A. 2012, *MNRAS*, 419, 573, doi: [10.1111/j.1365-2966.2011.19721.x](https://doi.org/10.1111/j.1365-2966.2011.19721.x)
- Mészáros, P., & Rees, M. J. 1997, *ApJL*, 482, L29, doi: [10.1086/310692](https://doi.org/10.1086/310692)
- Norris, J. P., Share, G. H., Messina, D. C., et al. 1986, *The Astrophysical Journal*, 301, doi: [10.1086/163889](https://doi.org/10.1086/163889)
- Panaitescu, A., Spada, M., & Mészáros, P. 1999, *The Astrophysical Journal*, 522, doi: [10.1086/312230](https://doi.org/10.1086/312230)
- Preece, R. D., Briggs, M. S., Mallozzi, R. S., et al. 2000, *The Astrophysical Journal Supplement Series*, 126, doi: [10.1086/313289](https://doi.org/10.1086/313289)
- Rees, M. J., & Meszaros, P. 1994, *The Astrophysical Journal*, 430, doi: [10.1086/187446](https://doi.org/10.1086/187446)
- Rybicki, G. B., & Lightman, A. P. 1979, *Radiative processes in astrophysics*
- Sakamoto, T., Barthelmy, S. D., Barbier, L., et al. 2008, *ApJS*, 175, 179, doi: [10.1086/523646](https://doi.org/10.1086/523646)

- Shen, R. F., & Zhang, B. 2009, *Monthly Notices of the Royal Astronomical Society*, 398,
doi: [10.1111/j.1365-2966.2009.15212.x](https://doi.org/10.1111/j.1365-2966.2009.15212.x)
- Takamoto, M. 2018, *MNRAS*, 476, 4263,
doi: [10.1093/mnras/sty493](https://doi.org/10.1093/mnras/sty493)
- Takamoto, M., Inoue, T., & Lazarian, A. 2015, *ApJ*, 815, 16, doi: [10.1088/0004-637X/815/1/16](https://doi.org/10.1088/0004-637X/815/1/16)
- Tavani, M. 1996, *The Astrophysical Journal*, 466,
doi: [10.1086/177551](https://doi.org/10.1086/177551)
- Thompson, C. 1994, *MNRAS*, 270, 480,
doi: [10.1093/mnras/270.3.480](https://doi.org/10.1093/mnras/270.3.480)
- Uhm, L. Z., Zhang, B., & Racusin, J. 2018, *The Astrophysical Journal*, doi: [10.3847/1538-4357/aab30](https://doi.org/10.3847/1538-4357/aab30)
- Uhm, Z. L., & Zhang, B. 2014, *Nature Physics*, 10, 351–356, doi: [10.1038/nphys2932](https://doi.org/10.1038/nphys2932)
- . 2016, *The Astrophysical Journal*, 825, 97,
doi: [10.3847/0004-637x/825/2/97](https://doi.org/10.3847/0004-637x/825/2/97)
- Usov, V. V. 1994, *MNRAS*, 267, 1035,
doi: [10.1093/mnras/267.4.1035](https://doi.org/10.1093/mnras/267.4.1035)
- Vetere, L., Massaro, E., Costa, E., Soffitta, P., & Ventura, G. 2006, *Astronomy and Astrophysics*, 447, 499,
doi: [10.1051/0004-6361:20053800](https://doi.org/10.1051/0004-6361:20053800)
- Yonetoku, D., Murakami, T., Nakamura, T., et al. 2004, *The Astrophysical Journal*, 609, doi: [10.1086/421285](https://doi.org/10.1086/421285)
- Yuan, W., Zhang, C., Ling, Z., et al. 2018, in *Space Telescopes and Instrumentation 2018: Ultraviolet to Gamma Ray*, ed. J.-W. A. den Herder, S. Nikzad, & K. Nakazawa, Vol. 10699, *International Society for Optics and Photonics (SPIE)*, 543 – 551,
doi: [10.1117/12.2313358](https://doi.org/10.1117/12.2313358)
- Zhang, B. 2018, *The Physics of Gamma-Ray Bursts*, doi: [10.1017/9781139226530](https://doi.org/10.1017/9781139226530)
- Zhang, B., & Mészáros, P. 2002, *ApJ*, 581, 1236,
doi: [10.1086/344338](https://doi.org/10.1086/344338)
- Zhang, B., & Pe’Er, A. 2009, *Astrophysical Journal*, 700, doi: [10.1088/0004-637X/700/2/L65](https://doi.org/10.1088/0004-637X/700/2/L65)
- Zhang, B., & Yan, H. 2011, *Astrophysical Journal*, 726, doi: [10.1088/0004-637X/726/2/90](https://doi.org/10.1088/0004-637X/726/2/90)
- Zhang, B., & Zhang, B. 2014, *Astrophysical Journal*, 782, doi: [10.1088/0004-637X/782/2/92](https://doi.org/10.1088/0004-637X/782/2/92)